Tidal barrage operational optimisation using wave energy control techniques

Available online at www.sciencedirect.com

ScienceDirect

IFAC Papers Online CONFERENCE PAPER ARCHIVE

IFAC PapersOnLine 55-31 (2022) 148–153

Tidal barrage operational optimisation using wave energy control techniques ⋆

John V. Ringwood * **Nicolás Faedo** **

* *Centre for Ocean Energy Research, Maynooth University, Ireland (e-mail: john.ringwood@mu.ie).*

** *Marine Offshore Renewable Energy Lab., Politecnico di Torino, Italy (e-mail: nicolas.faedo@polito.it)*

Abstract: Tidal barrages have been used as a source of renewable energy since Medieval times, though the commercial utilisation of tidal barrages for electricity production began in 1966. In the intervening time, a number of techniques have been used to optimise the operation of tidal barrages, in order to maximise their utility, against set criteria, usually including maximisation of converted energy. This paper examines what can be learned from a sister renewable energy application, wave energy, in terms of the energy-maximising control schemes employed. Specifically, comparisons are made in terms of the characteristics of the primary energy excitation, the set of control protocols available, and the mathematical models used to describe each system. In order to provide a preliminary assessment of the potential for the use of wave energy control concepts, a sample case study is undertaken, where a popular wave energy control philosophy is used to optimise the operation of a tidal barrage.

Keywords: Marine renewable energy, tidal barrages, wave energy, optimal control.

1. INTRODUCTION

Some of the earliest evidence of the use of tidal barrages to harness energy relates to the Medieval tidal barrages used to drive water wheels used, in turn, to drive mill wheels (Lobb et al., 2020; McErlean, 2007). More recently, 1966 saw the commissioning of the world's first commercial electricity generating tidal barrage, at La Rance in France (Frau, 1993) rated at 240 MW, and still in operation. Of the renewable resources, tidal energy provides a predictable, if intermittent, energy source and tidal barrage operation can be configured to focus more on maximisation of total tidal energy converted or spreading the energy more evenly over a particular (*e.g.* demand) interval Omitting twin-basin schemes from the present analysis, three basic operational modes for tidal barrages can be identified: (a) Generate only on ebb, (b) generate only on flood, and (c) Bi-directional generation. In general, bi-directional generate is more expensive (2-way turbines are required) and normally results in a lower overall energy take (due to the reduced range of variation within the basin) while, for uni-directional generation, ebb generation is preferred since, for flood generation, it involves using the basin between existing low tide level and slightly above normal mid-tide level, thus producing less energy (Hammons, 1993). More detailed operational possibilities are covered in Section 2, while broader aspects of tidal basin design are discussed by Prandle (2009).

A variety of published studies exist relating to the optimal operation of tidal barrages, with a useful overview presented by Hammons (1993), with more recent reviews by Waters and Aggidis (2016), Neill et al. (2018) and Angeloudis et al. (2021). Aggidis and Benzon (2013) undertake an operational assessment for a case study in the Mersey estuary, using a turbine model specified in Aggidis and Feather (2012), which has also been utilised by other researchers, including Angeloudis et al. (2018), who present two case studies for the Bristol Channel and Severn Estuary. Adopting a more formal optimal control approach, Ryrie (1995) and Shen and Nyman (2021) propose schemes based on Bellman's dynamic programming, and nonlinear model predictive control, respectively, while approaches utilising genetic optimisations are reported in (Neto et al., 2015; Xue et al., 2021).

In contrast to previous approaches, this paper proposes the use of control schemes developed within the wave energy control systems community (Ringwood et al., 2014; Faedo et al., 2017), specifically utilising the moment-based formulation of Faedo et al. (2018, 2021a), which has useful computational properties as well as the ability to handle linear and nonlinear system models. The remainder of the paper is organised as follows: Section 2 reviews the typical operational modes of tidal barrages and Section 3 examines their relationship with control modes typical of wave energy converters (WECs). A control-oriented mathmematical model for a tidal barrage is presented in Section 4, with a barrage operational control design, based on WEC control principles, following in Section 5. Conclusions are drawn in Section 6.

⋆ John Ringwood was supported by Science Foundation Ireland (SFI) through the MaREI Centre for Energy, Climate and Marine under Grant No. 12/RC/2302_P2, while Nicolás Faedo received funding from the European Union's Horizon 2020 Research and Innovation Programme under Marie Sklodowska-Curie grant agreement No. 101024372.

10.1016/j.ifacol.2022.10.423

2. BARRAGE OPERATIONAL MODES

The full set of possible barrage operational modes (adapted from (Angeloudis et al., 2018)), in a sequence corresponding to a full tidal cycle, are:

(1) Generating on tidal flood
(2) Free filling through sluices
(3) Pumping on flood to enhance basin water level
(4) Holding level in basin (sluices and turbine ducts closed)
(5) Generating on tidal ebb
(6) Free emptying through sluices
(7) Pumping on ebb to enhance emptying of basin
(8) Holding level in basin (sluices and turbine ducts closed)

Note that (1) and/or (2) and (5) and (6) can possibly be combined (*e.g.* partial overlap) and it can be noted that operation of any particular barrage may skip a number of the steps listed above, apart from at least (1) or (5). Fig.1 shows a complete cycle of tidal barrage operation, including all the steps in the above sequence.

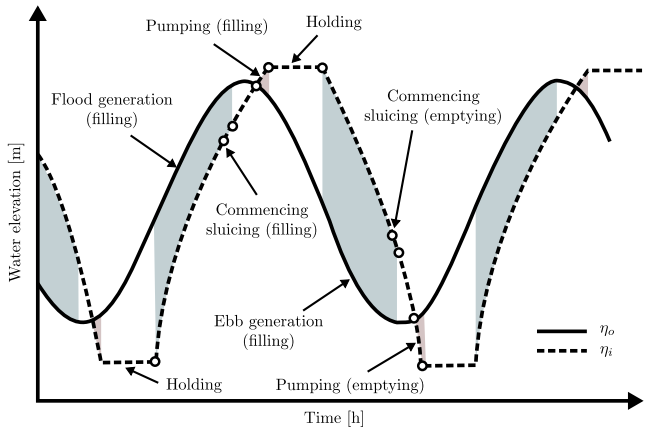

Fig. 1. Full set of barrage control modes, with overlapping generation/sluicing (Angeloudis et al., 2018). η_i represents the internal (basin) water level, while η_o is the outside (external) water level.

3. BARRAGE AND WEC CONTROL COMPARISON

In the same way that tidal barrages are subject to sinusoidal (tidal) waves, WECs are also subject to wind-generated sea waves, containing a spread of wave frequencies, normally corresponding to a wave spectrum (in our consideration of WECs, we will focus on the resonant point-absorber [PA] case). Nevertheless, a variety of wave energy control philosophies were originally developed for monochromatic excitation, as a starting point, including a number of 'discrete' control algorithms such as latching and declutching (Clément and Babarit, 2012), which perform an essentially similar function to 'holding' and 'sluicing' in the barrage parlance. These actions, in both domains, serve to increase the buildup of potential energy (latching/holding) or increase the momentum in movement (declutching/sluicing). However, one important difference exists, in that the control actions undertaken in tidal barrage operation affect the subsequent level of excitation available, which is not the case in the wave energy application. One other general distinction is that tidal barrage systems represent highly damped dynamical systems, due to the restriction in fluid movement between the basin and the open ocean, either via turbines or sluicing. These restrictions significantly dampen the resonance effect responsible for the often spectacular increase in height of the tidal wave in estuaries; for example the Severn estuary has a tidal range of ≈ 12 [m], while the mean open ocean tidal range is ≈ 0.6 [m]. In contrast, many wave energy devices, for example point absorbers, are highly resonant, though some (*e.g.* oscillating wave surge converters) are less so, essentially acting as wave followers.

In terms of a direct comparison, probably the closest WEC class to a tidal barrage system is the oscillating water column (OWC), where movement of the water itself (inside a chamber) is used to power a bi-directional *air* turbine, though some trials have also been made with water-based turbines (Hashem et al., 2018). However, a major advantage of tidal barrages is the unidirectional motion of the water over a long period, while OWCs require bi-directional (Wells, impulse, bi-radial) turbines with relatively low efficiency to rectify the fast reciprocating water/air flow of wind-generated waves. A final point of comparison between WECs and tidal barrage operations is the use of grid power to enhance the overall energy captured, over a wave cycle. In the WEC case, this is termed *reactive* control (Ringwood et al., 2014), where power is injected into the system at specific points in the cycle, enhancing the motion and increasing the overall energy captured. In the tidal barrage case, pumping is used when the levels inside and outside the barrage are relatively close, incurring a low power (hydraulic head) overhead, but reaping the reward when the water level outside the barrage changes substantially.

Given these obvious associations between (some) wave energy systems and tidal barrages, an attempt is made in Table 1 to draw some direct comparisons between the operational actions, and terminology, used in these disparate ocean energy applications, following the modal labels in Section 2.

Table 1. Equivalence between operational modes in tidal barrages and wave energy operation/control.

Mode	Tidal barrage	WEC
1	Generating on flood	Generating on rise
2	Free filling	Declutching
3	Pumping (fill)	Reactive raise
4	Holding (high level)	Latching
5	Generating on ebb	Generating on fall
6	Free emptying	Declutching
7	Pumping (emptying)	Reactive lower
8	Holding (low level)	Latching

During barrage generation, there are also possibilities (either through pitch control of the turbines, or generator torque), to vary the level of 'load', or damping, which the water flow is subject to, though this may not be as useful a control input as in the WEC case. In essence, the instantaneous power generated is the velocity-torque product:

$$P(t) = v(t)T(t), \tag{1}$$

with, of course, captured energy, over an interval $0 \to t^*$ being:

$$E(t^*) = \int_0^{t^*} P(t)\mathrm{d}t, \tag{2}$$

so it makes sense to control the generator torque to maximise (1). In the WEC application, torque is typically used as the primary manipulated control variable. In terms of any of declutching, latching, or continuous torque control, the optimal solution, for a WEC described by linear hydrodynamics, is symmetrical *i.e.* the solutions for upward and downward motion are the exact inverse of each other. This is true since the wave excitation is not, in general, a function of any previous control actions. For the barrage case, since the degree of filling of the basin is, itself, a function of the control actions carried out over the filling half-cycle, the optimal control solution may not be symmetrical.

Finally, an aspect that defines both barrage and WEC control problems is the presence of physical constraints, which need to be handled as part of the control solution. For the WEC case, typical physical constraints include limits on generator torque, and WEC displacement and velocity. For the barrage case, there are limits on (sluice) filling and emptying rates (or, more correctly, maximum sluice area), generator torque, and maximum and minimum basin water levels.

4. BARRAGE MATHEMATICAL MODEL

For simplicity, in this analysis, we will assume that the basin is regular in shape (*e.g.* a right-angle prism), so that the basin volume is a simple function of the basin water level (a 0-D model). Neglecting losses, the potential energy E_p due to a hydraulic head H, developed across a tidal barrage, is quantified (Prandle, 2009) as [1]:

$$E_p = \frac{1}{2}\rho g A H^2, \tag{3}$$

where ρ is the water density, g is the acceleration due to gravity, and A the impounded surface area, assuming uniform depth, while:

$$H(t) = \eta_i(t) - \eta_o(t), \tag{4}$$

with η_i being the basin (inside) water level and $\eta_o = A_t \cos(\omega_t t)$ ($\omega_t = \frac{2\pi}{T_t}$, with T_t the tidal period) the outside (open ocean) water level. Again, for simplicity, we will assume that the tidal range A_t is constant *i.e.* neglecting spring/neap or other longer term variations.

Given a flow through the barrage Q, which could be through all possible openings (turbine ducts/caissons or sluice gates), the change in basin water level is:

$$A_b \dot{\eta}_i(t) = -Q(t), \tag{5}$$

where A_b is the basin surface area profile, assumed constant (i.e. the basin has vertical walls) and Q is the total instantaneous flow from the basin to the open sea, resulting from flow through the turbines Q_t and flow through the sluice gates Q_s, so that:

$$Q = Q_t + Q_s, \tag{6}$$

[1] From now on, the dependence on t is omitted when clear from the context.

4.1 Generation

The instantaneous hydraulic power, available through the turbines, is:

$$P_h = \rho g H Q_t, \tag{7}$$

and the extracted energy, over an interval $\Omega = [t_1, t_2] \subset \mathbb{R}^+$, during power generation is:

$$E_e = \rho g \int_\Omega H(t) Q_t(t)\mathrm{d}t. \tag{8}$$

4.2 Sluicing

The flow through a fully submerged sluice gate of area A_s is:

$$Q_s(t) = \epsilon\sqrt{2gH(t)}A_s(t), \tag{9}$$

where ϵ is a contraction (discharge) coefficient. We note that no power is generated by flooding or discharge through the sluice gates. They merely provide a possibility to accelerate the rate of filling/emptying of the basin to increase the hydraulic head during a subsequent tidal half cycle.

4.3 Overall model

The full system model, for the purposes of this study, can now be specified as:

$$A_b\dot{\eta}_i = -Q_t - \epsilon\,\mathrm{sign}(\eta_i - \eta_o)\sqrt{2g\,|\eta_i - \eta_o|}A_s, \tag{10}$$

defined in terms of the total flow into, or out of, the basin, using Q_t and A_s as manipulated (control) variables. Since Q_t can be positive or negative, irrespective of the sign of the hydraulic head ($\mathrm{sign}(\eta_i - \eta_o)$), the turbines can be either generating, or pumping.

5. BARRAGE OPTIMAL OPERATION USING WEC CONTROL

5.1 Definition of the optimal control problem

Analogously to the wave energy case, we can formally define the so-called *energy-maximising* optimal control problem (OCP) for tidal barrage operation as follows. For any given external (outside) tidal variation input tide η_o, find an optimal pair (Q_t, A_s) such that the corresponding mean hydraulic energy absorption (derived from (8)) is maximised, *i.e.* the OCP can be defined in terms of the problem (P) as:

$$\begin{aligned}
&(P):\\
&(Q_t^{\mathrm{opt}}, A_s^{\mathrm{opt}}) = \arg\max_{(Q_t, A_s)} \frac{\rho g}{T_t}\int_\Omega (\eta_i - \eta_o)Q_t\mathrm{d}t,\\
&\text{subject to:}\\
&A_b\dot{\eta}_i = -Q_t - \epsilon\,\mathrm{sign}(\eta_i - \eta_o)\sqrt{2g\,|\eta_i - \eta_o|}A_s,\\
&|\eta_i| \le N_i^{\max} \quad \text{(basin water level limits)},\\
&|Q_t| \le Q_t^{\max} \quad \text{(turbine flow limits)},\\
&0 \le A_s \le A_s^{\max} \quad \text{(sluice gate opening limits)},
\end{aligned} \tag{11}$$

for $t \in \Omega \subset \mathbb{R}^+$, with $\Omega = [0, T_t]$, being T_t the tide period (see Section 4), and where the set $\{N_i^{\max}, Q_t^{\max}, A_s^{\max}\} \subset \mathbb{R}^+$ defines the (controlled) system limitations, in terms of appropriate state and input constraints.

5.2 Direct optimal moment-based control

Given the similitudes between WEC optimal control and optimal tidal barrage operation, as exposed and discussed throughout Section 3, we propose to borrow techniques from the former control design problem to solve the tidal barrage OCP (P) in (11). In particular, we adopt the so-called *moment-based* approach, as developed through a series of WEC control studies (see *e.g.* Faedo et al. (2021a, 2020)). Moment-based control is heavily based upon the notion of a *moment*, interpreted from a system theoretic perspective (see *e.g.* Astolfi (2010)).

In particular, moment-based control is based upon the idea of transcribing the OCP (11) into a finite-dimensional nonlinear program (NP) by making explicit use of moments. If the transcription is effectively well-posed, the resulting NP can be solved numerically using state-of-the-art solvers. Although we do not provide a full account on moment-based theory in this paper, we briefly expose the main ideas towards direct transcription of problem (P) via moments in the following paragraphs.

As a first step, let us define the tidal barrage external input, *i.e.* the wave tide η_o, in terms of a suitable implicit form description. In particular, we define the following *signal generator* $\mathscr{G}$ (sometimes referred to as *exogeneous system*), for $t \in \mathbb{R}^+$, in terms of the set of first-order differential equations

$$\mathscr{G}: \begin{cases} \dot{\theta} = S\theta, \\ \eta_o = L_{\eta_o}\theta, \end{cases} \quad S = 0 \oplus \begin{bmatrix} 0 & \omega_t \\ -\omega_t & 0 \end{bmatrix}, \tag{12}$$

with a given intial condition $\theta(0) \in \mathbb{R}^3$ such that the pair $(S, \theta(0))$ is reachable, and where the output vector, defining η_o in (12), is such that $L_{\eta_o}^{\mathsf{T}} \in \mathbb{R}^3$. We recall that the value $\omega_t = 2\pi/T_t$ denotes the tide frequency, which acts as the so-called *fundamental frequency* of η_o.

Note that the family of functions generated by (12) are those belonging to $\mathscr{X} = \text{span}\{1, \cos(\omega_t t), \sin(\omega_t t)\}$, which is effectively consistent with the nature of η_o described within Section 4. Although, from now on, we assume η_o is a zero-mean map (consistent with Section 4), the constant function $\{1\}$ in $\mathscr{X}$ is included to cater for any possible deviation in mean value when computing the optimal gate area A_s, which is required to enforce the non-symmetrical sluicing constraints in the definition of the OCP (P) (11).

Although the implicit description in (12) effectively provides an exact account of the map η_o, the control variables to be optimised, *i.e.* the pair (Q_t, A_s), are not (in general) described accurately by means of (12). With the standard assumption that $\{Q_t, A_s\} \subset L^2(\Omega)$, we adopt from Faedo et al. (2021a,b) the following approximate implicit description, based upon a corresponding extension of (12). In particular, let us define the so-called *extended signal generator* $\overline{\mathscr{G}}$, which 'extends' $\mathscr{G}$ in (12) in the following sense:

$$\overline{\mathscr{G}}: \begin{cases} \dot{\overline{\theta}} = \overline{S\theta}, \\ Q_t = \overline{L_{Q_t}\theta}, \\ A_s = \overline{L_{A_s}\theta}, \\ \eta_o = \overline{L_{\eta_o}\theta}, \end{cases} \quad \overline{S} = S \oplus \left(\bigoplus_{p=2}^{d} \begin{bmatrix} 0 & p\omega_t \\ -p\omega_t & 0 \end{bmatrix} \right), \tag{13}$$

with $\overline{S} \in \mathbb{R}^{\iota \times \iota}$, $\iota = 2(d+1)+1$, and where the set of vectors $\{\overline{L_{Q_t}}^{\mathsf{T}}, \overline{L_{A_s}}^{\mathsf{T}}, \overline{L_{\eta_o}}^{\mathsf{T}}\} \subset \mathbb{R}^{\iota}$. Note that, given the nature of the matrix $\overline{S}$ in (13), the output vector $\overline{L_{\eta_o}}$, defining the tide η_o, is simply the result of an appropriate inclusion:

$$\eta_o = L_{\eta_o}\theta = [L_{\eta_o}\, 0]\,\overline{\theta} = \overline{L_{\eta_o}\theta}, \tag{14}$$

with the specific map being $\mathcal{I} : \mathbb{R}^{1\times 3} \hookrightarrow \mathbb{R}^{1\times \iota}$, $\mathcal{I}(L_{\eta_o}) \mapsto \overline{L_{\eta_o}}$. Furthermore, the initial condition of (13) can be defined in terms of $\theta(0)$ simply as $\overline{\theta}(0)^{\mathsf{T}} = [\xi(0)^{\mathsf{T}}\, \theta_{\text{e}}(0)^{\mathsf{T}}]$, with any vector $\theta_{\text{e}}(0) \in \mathbb{R}^{2d}$ such that $(\overline{S}, \overline{\theta}(0))$ is reachable.

Suppose, without any loss of generality, that the initial condition of the extended signal generator (13) is set to $\overline{\theta}(0)^{\mathsf{T}} = [1\ \varepsilon_{\iota}^{\mathsf{T}}]^{\mathsf{T}}$, so that the pair of matrices $(\overline{S}, \overline{\theta}(0))$ is effectively reachable. Under the implicit description posed in (13) there exists (see *e.g.* Astolfi (2010); Faedo et al. (2021b)) a mapping π such that, for any fixed trajectory $\theta(t)$ of $\overline{\mathscr{G}}$, the steady-state response η_i^{ss} of (5) is $\eta_i^{\text{ss}}(t) = \pi(\overline{\theta}(t))$. The mapping π is termed the *moment* of (5) at the signal generator (13).

Following Faedo et al. (2021a,b), an approximation of the moment π can be computed, for any ι in (13) sufficiently large, in terms of a finite-dimensional approximation over the set spanned by $\{\overline{\theta}_i\}_{i=1}^{\iota}$, *i.e.*

$$\pi(\overline{\theta}) \approx \overline{L_{\eta_i}\theta}, \tag{15}$$

with $\overline{L_{\eta_i}} \in \mathbb{R}^{\iota}$ and, hence, for any given trajectory $\overline{\theta}(t)$ the steady-state behaviour η_i^{ss} can be correspondingly approximated as

$$\eta_i^{\text{ss}}(t) \approx \overline{\eta_i}(t) = \overline{L_{\eta_i}}\overline{\theta}(t). \tag{16}$$

Following the ideas exposed in Faedo et al. (2021a,b), the specific computation $\overline{L_{\eta_i}}$, which is instrumental for the results presented in the reminder of this section, can be computed in terms of a Galerkin-like procedure. To be precise, by noting that

$$\dot{\overline{\eta_i}} = \overline{L_{\eta_i}\dot{\theta}} = \overline{L_{\eta_i}S\theta}, \tag{17}$$

by virtue of (13), we can define the following *residual* map $\mathscr{R} : \mathbb{R}^+ \to \mathbb{R}$ as

$$\mathscr{R} := \left(A_b S\overline{L_{\eta_i}} + \overline{L_{Q_t}}\right)\overline{\theta} + \left(\epsilon\, \text{sign}\left((\overline{L_{\eta_i}} - \overline{L_{\eta_o}})\overline{\theta}\right)\sqrt{2g\left|(\overline{L_{\eta_i}} - \overline{L_{\eta_o}})\overline{\theta}\right|}\right)\overline{L_{A_s}\theta}, \tag{18}$$

which arises of 'replacing' $\{\eta_o, \eta_i, Q_t, A_s\}$ by their corresponding moment-based descriptions, *i.e.* in terms of the solution of the signal generator (13). Considering the standard inner-product in $L^2(\Omega)$, for any given triple $(\overline{L_{\eta_o}}, \overline{L_{Q_t}}, \overline{L_{A_s}})$ and any ι sufficiently large, we can compute $\overline{L_{\eta_i}}$ in (16) as the solution of the (nonlinear) system of algebraic equations

$$\left\langle \mathscr{R}, \overline{\theta}^{\mathsf{T}} \right\rangle = 0 \to \overline{\mathscr{R}}(\overline{L_{\eta_o}}, \overline{L_{\eta_i}}, \overline{L_{Q_t}}, \overline{L_{A_s}}) = 0, \tag{19}$$

corresponding with the projection of the residual map (18) onto the function space spanned by the set $\{\overline{\theta}_i\}_{i=1}^{\iota}$, and where $(\overline{L_{\eta_o}}, \overline{L_{\eta_i}}, \overline{L_{Q_t}}, \overline{L_{A_s}}) \mapsto \overline{\mathscr{R}}((\overline{L_{\eta_o}}, \overline{L_{\eta_i}}, \overline{L_{Q_t}}, \overline{L_{A_s}}))$ denotes the map induced by such operation.

With the definitions provided up until this point, we can make the following observation. Using the corresponding moment-based descriptions, the integral operation within

the objective function characterising (P) can be mapped (see Faedo et al. (2018, 2021a)) as

$$\begin{aligned}\int_\Omega (\eta_i - \eta_o) Q_t \mathrm{d}t &\mapsto \int_\Omega (\overline{L_{\eta_i}}\theta - \overline{L_{\eta_o}}\theta)(\overline{L_{Q_t}}\theta)\mathrm{d}t \\ &\mapsto \frac{T_t}{2}(\overline{L_{\eta_i}} - \overline{L_{\eta_o}})\overline{L_{Q_t}}^{\mathsf{T}},\end{aligned} \tag{20}$$

and hence the infinite-dimensional OCP (P) in (11) can be approximated in terms of the following moment-based NP

$$\begin{aligned}&\widetilde{(P)}: \\ &(\overline{L_{Q_t}}^{\mathrm{opt}}, \overline{L_{A_s}}^{\mathrm{opt}}) = \arg \max_{(\overline{L_{Q_t}}, \overline{L_{A_s}})} \frac{\rho g}{2}(\overline{L_{\eta_i}} - \overline{L_{\eta_o}})\overline{L_{Q_t}}^{\mathsf{T}}, \\ &\text{subject to:} \\ &\overline{\mathscr{R}}(\overline{L_{\eta_o}}, \overline{L_{\eta_i}}, \overline{L_{Q_t}}, \overline{L_{A_s}}) = 0, \\ &\overline{L_{\eta_i}}\mathscr{A}_{\eta_i} \leq \mathscr{B}_{\eta_i}, \\ &\overline{L_{Q_t}}\mathscr{A}_{Q_t} \leq \mathscr{B}_{Q_t}, \\ &\overline{L_{A_s}}\mathscr{A}_{A_s} \leq \mathscr{B}_{A_s},\end{aligned} \tag{21}$$

where the pairs of matrices $(\mathscr{A}_{\eta_i}, \mathscr{B}_{\eta_i})$, $(\mathscr{A}_{Q_t}, \mathscr{B}_{Q_t})$, and $(\mathscr{A}_{A_s}, \mathscr{B}_{A_s})$ correspond with the direct (time) collocation of the set of state and input inequality constraints in (11) within a finite set of $N_c \in \mathbb{N}$ instants $\mathcal{T} = \{t_i\}_{i=1}^{N_c} \subset \Omega$ (see *e.g.* Faedo et al. (2018, 2021a)).

5.3 Example case

To provide a brief numerical example case on the application of the moment-based control procedure, outlined in Section 5.2 and formalised in problem $\widetilde{(P)}$, we consider a tidal barrage consistent with the so-called Cumberland Basin (see Prandle (1984)), located in the Bay of Fundy, Canada. The specific parameters, characterising the case study under consideration, are summarised in Table 2. Note that the maximum flow $Q_t^{\max}$ has been chosen, for this numerical appraisal, as approximately five times the rated flow reported in Prandle (1984) for this basin.

Table 2. Parameter specification for the example case, adopted from Prandle (1984).

Parameter	Value
Basin surface area A_b	86.2 [km^2]
Tidal amplitude A_t	3 [m]
Tidal period T_t	12.42 [h]
Discharge coefficient ϵ	1
Max. basin level $N_i^{\max}$	3 [m]
Max. turbine flow $Q_t^{\max}$	6000 [m^{3}s^{-1}]
Max. gate area $A_s^{\max}$	7893 [m^2]

With respect to the specifics regarding the direct transcription of the associated OCP (P) into the moment-based NP $\widetilde{(P)}$, the order of the extended signal generator (13) is chosen with $d = 30$, *i.e.* 30 (super) harmonics of the fundamental (tide) frequency ω_t are chosen to compute a moment-based approximation of the optimal control variables Q_t and A_s accordingly. The set $\mathcal{T}$, used to enforce the set of state and input inequality constraints in (21), is chosen to be uniformly distributed in Ω, with a step of

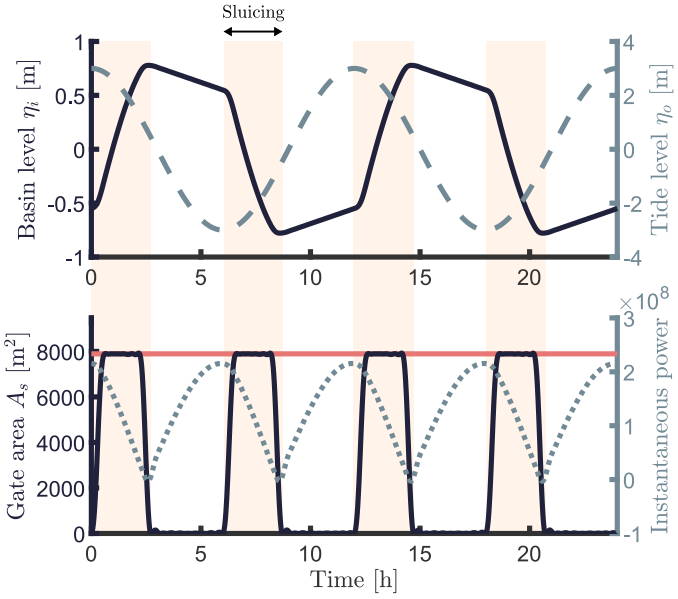

Fig. 2. Top: optimally controlled basin level η_i (left axis, solid line), and the corresponding tide level η_o (right axis, dashed line). Bottom: optimally controlled change in gate area A_s (left axis, solid line), and instantaneous hydraulic power (right axis, dotted line). The maximum gate area is indicated with a red horizontal line.

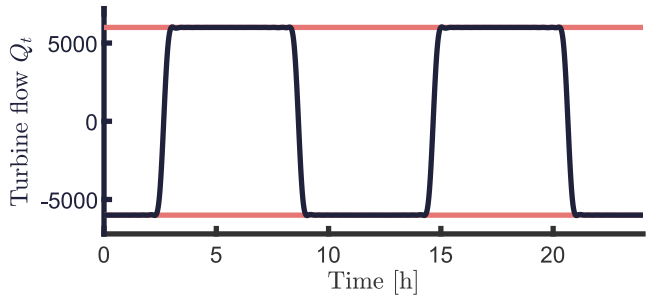

Fig. 3. Optimal turbine flow. The limits on turbine flow are indicated with red horizontal lines.

0.1 [h]. The resulting NP $\widetilde{(P)}$ is solved via interior-point methods.

Fig. 2 (top) presents the optimally controlled basin level η_i (left axis, solid line), and the corresponding tide level η_o (right axis, dashed line), with an amplitude of 3 [m], while Fig. 2 (bottom) shows optimally controlled change in gate area A_s (left axis, solid line), and instantaneous hydraulic power (right axis, dotted line). It can be appreciated that the optimal profile for the variation in gate area adopts an (approximate) bang-bang-type behaviour, *i.e.* the gates are either fully open (with a maximum limit defined by $A_s^{\max}$), or fully closed ($A_s = 0$), which is consistent with that qualitatively reported in Prandle (1984). Note that, for this particular tide η_o, the basin level never reaches its constraint limit (set to 3 [m] - see Table 2), since the corresponding basin area is significantly large, and neither the optimal gate action, nor the optimal turbine input flow (or their effective combination), is sufficient to fully exploit the imposed maximum level. This (at least partially) explains the bang-bang-type behaviour also

present for the optimal turbine flow in Fig. 3. Note that both optimally controlled A_s and Q_t thoroughly respect the imposed limitations by virtue of the moment-based solution proposed. Finally, though beyond the scope of this paper, we note that a different solution class (with a slower rate of change) might be expected if either: a) the basin area is smaller; or b) the limits in turbine flow and maximum gate area are less restrictive.

6. CONCLUSION

This paper demonstrates that optimal control of tidal barrages can be approached using techniques borrowed from wave energy control; specifically, there is a close association between the problems of barrage control and the control of wave energy devices in monochromatic seas. Though the terminology is quite different, the control functions of holding (latching), generating (loading), sluicing (declutching), and pumping (reactive control) all have equivalences between the two applications. The WEC control formulation also offers the designer a formal framework to solve the problem and can effectively and efficiently deal with constraints on basin level, maximum sluicing aperture, and maximum flowrate through the turbines.

Though this preliminary study has a number of limiting assumptions (e.g. a single monochromatic semi-diurnal tidal period, an assumed independence between turbine flow rate and hydraulic head, and vertical tidal basin walls), it provides a pathway to further examine the tidal barrage control problem within a mathematical framework developed predominantly for wave energy applications. Future research will focus on the use of more realistic models for both barrage and exciting force.

REFERENCES

Aggidis, G. and Benzon, D. (2013). Operational optimisation of a tidal barrage across the mersey estuary using 0-d modelling. *Ocean Engineering*, 66, 69–81.

Aggidis, G. and Feather, O. (2012). Tidal range turbines and generation on the Solway Firth. *Ren. Energy*, 43, 9–17.

Angeloudis, A., Kramer, S.C., Avdis, A., and Piggott, M.D. (2018). Optimising tidal range power plant operation. *Applied Energy*, 212, 680–690.

Angeloudis, A., Mackie, L., and Piggott, M.D. (2021). Tidal range energy.

Astolfi, A. (2010). Model reduction by moment matching for linear and nonlinear systems. *IEEE Transactions on Automatic Control*, 55(10), 2321–2336.

Clément, A. and Babarit, A. (2012). Discrete control of resonant wave energy devices. *Phil. Trans. of the Royal Soc. A: Math., Phys. and Eng. Sc.*, 370(1959), 288–314.

Faedo, N., Olaya, S., and Ringwood, J.V. (2017). Optimal control, MPC and MPC-like algorithms for wave energy systems: An overview. *IFAC J. of Syst. and Con.*, 1, 37–56.

Faedo, N., Peña-Sanchez, Y., and Ringwood, J.V. (2020). Receding-horizon energy-maximising optimal control of wave energy systems based on moments. *IEEE Transactions on Sustainable Energy*, 12(1), 378–386.

Faedo, N., Scarciotti, G., Astolfi, A., and Ringwood, J.V. (2018). Energy-maximising control of wave energy converters using a moment-domain representation. *Control Engineering Practice*, 81, 85–96.

Faedo, N., Scarciotti, G., Astolfi, A., and Ringwood, J.V. (2021a). Nonlinear energy-maximizing optimal control of wave energy systems: A moment-based approach. *IEEE Transactions on Control Systems Technology*, 29(6), 2533–2547.

Faedo, N., Scarciotti, G., Astolfi, A., and Ringwood, J.V. (2021b). On the approximation of moments for nonlinear systems. *IEEE Transactions on Automatic Control*, 66(11), 5538–5545.

Frau, J.P. (1993). Tidal energy: promising projects: La rance, a successful industrial-scale experiment. *IEEE Transactions on Energy Conversion*, 8(3), 552–558.

Hammons, T.J. (1993). Tidal power. *Proceedings of the IEEE*, 81(3), 419–433.

Hashem, I., Hameed, H.A., and Mohamed, M. (2018). An axial turbine in an innovative oscillating water column (owc) device for sea-wave energy conversion. *Ocean Engineering*, 164, 536–562.

Lobb, M., Brown, T., Leyland, J., Bernard, V., Daire, M.Y., and Langouët, L. (2020). An estuarine tidescape of production: terrestrial laser scanning of fixed fishing structures and a tide mill in the léguer estuary, brittany. *Antiquity*, 94(377), 1296–1313.

McErlean, T. (2007). *Harnessing the Tides, The Early Medieval Tide Mills at Nendrum Monastery, Strangford Lough, N. Ireland Arch. Monographs No 7.*

Neill, S.P., Angeloudis, A., Robins, P.E., Walkington, I., Ward, S.L., Masters, I., Lewis, M.J., Piano, M., Avdis, A., Piggott, M.D., et al. (2018). Tidal range energy resource and optimization–past perspectives and future challenges. *Renewable Energy*, 127, 763–778.

Neto, P.B.L., Saavedra, O.R., and Ribeiro, L.A.S. (2015). Optimization of electricity generation of a tidal power plant with reservoir constraints. *Ren. Energy*, 81, 11–20.

Prandle, D. (1984). Simple theory for designing tidal power schemes. *Adv. in water resources*, 7(1), 21–27.

Prandle, D. (2009). Design of tidal barrage power schemes. In *Proceedings of the Institution of Civil Engineers-maritime Engineering*, volume 162, 147–153.

Ringwood, J.V., Bacelli, G., and Fusco, F. (2014). Energy-maximizing control of wave-energy converters: The development of control system technology to optimize their operation. *IEEE Control Syst. Mag*, 34(5), 30–55.

Ryrie, S. (1995). An optimal control model of tidal power generation. *Applied Math. modelling*, 19(2), 123–126.

Shen, Y. and Nyman, P.O. (2021). Optimal operation of tidal plants based on nonlinear model predictive control strategy. In *IOP Conference Series: Earth and Environmental Science*, volume 687, 012101.

Waters, S. and Aggidis, G. (2016). Tidal range technologies and state of the art in review. *Renewable and Sustainable Energy Reviews*, 59, 514–529.

Xue, J., Ahmadian, R., Jones, O., and Falconer, R.A. (2021). Design of tidal range energy generation schemes using a genetic algorithm model. *Applied Energy*, 286, 116506.